

# Design and Development of a Novel Compact Soft-Surface Structure for the Front-to-Back Ratio Improvement and Size Reduction of a Microstrip Yagi Array Antenna

Trang T. Thai, *Student Member, IEEE*, Gerald R. DeJean, *Member, IEEE*, and Manos M. Tentzeris, *Senior Member, IEEE*

**Abstract**—In this letter, a novel antenna structure based on a microstrip Yagi array antenna and a soft surface (SS) ring is proposed, that enables a highly directional gain in addition to an improved front-to-back (F/B) ratio of more than 20 dB. The SS ring is shown to be capable of greatly improving the performance while miniaturizing the design's size by half. The implementation of the SS ring to a microstrip Yagi array antenna is demonstrated to verify its functionality in suppressing surface waves, showing that an improvement of at least 3 dB in the F/B ratio can be obtained. The design is investigated at the center frequency of 5.8 GHz; however, the structure can be easily scaled to other frequency ranges. A design analysis is performed to give insight into the operational mechanism of the SS ring and the critical dimensions that affect the SS structure surrounding the antenna array. In addition, measurements are presented to validate the results obtained via simulation. The principles established in this letter can be applied to other planar antenna designs.

**Index Terms**—Front-to-back (F/B) ratio, microstrip Yagi array, radiation-pattern improvement, soft surface.

## I. INTRODUCTION

**D**IRECTIONAL antenna arrays are becoming a necessary requirement for many wireless local area network (WLAN) applications to suppress unwanted interference and to optimize power efficiency and coverage range. Since Yagi-Uda antennas operate as endfire arrays [1], they have been utilized in numerous applications where directional radiation is necessary for long-distance wireless and point-to-point communications.

However, Yagi arrays have certain disadvantages such as size. These sometimes bulky structures can become unsuitable for compact integration with microwave monolithic integrated circuits (MMICs) and RF circuitry due to their size [2], [3]. Various efforts attempting to combine the directional characteris-

tics of the Yagi arrays with the advantages of microstrip antennas, namely printed Yagi antennas, have been proposed over the last 15 years [4]–[7]. Unfortunately, the tradeoff between gain and F/B ratio remains an area of concern. Different techniques have been proposed and utilized to improve the gain and F/B ratio of the microstrip Yagi antennas, including the use of periodic bandgap (PBG) structures [7] and conventional soft-hard surface (SHS) structures [8] that may require complicated and costly fabrication processes.

In this letter, we propose a new configuration that is based on the antenna in [9] implemented with a soft surface (SS) ring, that can improve the F/B ratio by at least 3 dB, while maintaining high-gain, low-sidelobe level, and low-cross polarization as well as sustaining high F/B ratio over a wider bandwidth. In contrast to the conventional SHS which is difficult to manufacture and requires a large area [10], the innovative SS structure consists of quarter-wavelength metal strips that are short-circuited to the ground plane. This concept of the modern SS allows for a robust implementation and a simple fabrication process with standard double-sided copper (Cu) clad boards.

## II. IMPLEMENTATION OF THE SS STRUCTURE

The concept of SHS was first considered by Kildal in [11] but modified in this letter to achieve optimal performance. Fig. 1 shows a schematic of the structure. The design consists of a compact SS rectangular ring,  $S_i$ , made of metal strips that are shorted to the ground plane through metallized walls,  $S_w$ , which are placed along the outer edge of the metal strips. In fabrication, the metal walls are realized by utilizing metal vias. All the metal strips have the same optimized width, denoted  $Q_s$ , which is  $\lambda_g/4$  where  $\lambda_g$  is the guided wavelength ( $\lambda_g = \lambda_o/\epsilon_{\text{eff}}^{0.5}$  where  $\epsilon_{\text{eff}}$  is the effective dielectric constant with a value between 1 and  $\epsilon_r$ , and  $\lambda_o$  is the free space wavelength). The inner width of the SS ring,  $W_s$ , is approximately one  $\lambda_o$ . The inner length of the SS ring,  $L_s$ , is approximately  $1.7\lambda_o$ . The dimensions of the antenna are denoted by the following variables: the length and width of the driven element, “D”, are  $L_D$  and  $W_D$ , respectively; the lengths and widths of director 1, “D1”, and director 2, “D2”, are  $L_{D1}$ ,  $W_{D1}$ ,  $L_{D2}$  and  $W_{D2}$ , respectively; and the length and width of the reflector, “R”, are  $L_R$  and  $W_R$ , respectively. The physical dimensions are as follows (in mils):  $L_R = 223$ ,  $W_R = 914$ ,  $L_D = 629$ ,  $W_D = 674$ ,  $L_{D1} = L_{D2} = 610$ ,  $W_{D1} = W_{D2} = 448$ ,  $L_S = 3484$ ,  $W_S = 2242$ ,  $Q_S = 332$ ,

Manuscript received April 18, 2008; revised May 31, 2008. Current version published November 12, 2008. This work was supported by the Georgia Electronic Design Center.

T. T. Thai is with the School of Electrical and Computer Engineering, Georgia Institute of Technology, Atlanta 30332, USA (e-mail: trang.thai@gatech.edu).

G. R. DeJean is with the Microsoft Research, Redmond, WA 98052 USA (e-mail: dejean@microsoft.com).

M. M. Tentzeris is with the Georgia Electronic Design Center, School of Electrical and Computer Engineering, Georgia Institute of Technology, GA 30332 USA (e-mail: etentze@ece.gatech.edu).

Color versions of one or more of the figures in this letter are available online at <http://ieeexplore.ieee.org>.

Digital Object Identifier 10.1109/LAWP.2008.2001818

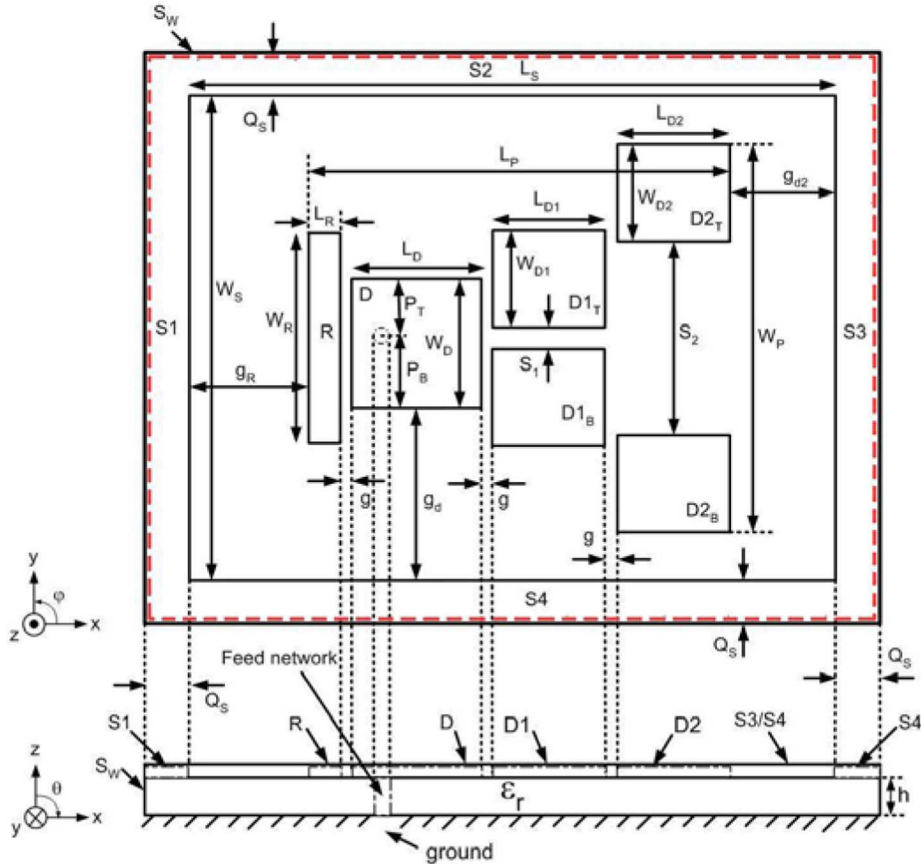


Fig. 1. Two-dimensional view of the SS microstrip Yagi array antenna.

$p_B = 377$ ,  $p_T = 297$ ,  $g_R = 558$ ,  $g_d = 784$ , and  $g_{d2} = 758$ . The resonant frequency is 5.8 GHz, and the lateral size of the ground (and substrate) is  $4135 \times 2904$  mils.

### III. PRINCIPLES OF OPERATION

The mechanism for the improvement in the radiation characteristics of the antenna is achieved by two main factors. The first is the surface wave suppression achieved by the high impedance of the SS ring that blocks the power flow normal to its surface. This is a well known factor that will not be discussed in this letter. Readers are directed to [10] and [11] for a detailed explanation of this effect. The roles of S1, S2, S3, and S4 have equally significant contributions because together they form an open-circuit boundary that gives the high impedance effect. The second factor is attributed to array coupling between the SS metal strips and the driven and director patches of the antenna. In particular, the two SS metal strips in the x-direction together with the driven element and the director D1 and D2 patches form a five-element array that further improves the radiation in the quasi-endfire direction (quadrant I). Due to the constructive interference of the  $R - D - D1_T - D2_T$  and the  $R - D - D1_B - D2_B$  single microstrip Yagi arrays [9], the two directors,  $D1_T$  and  $D1_B$  patches are considered as a single effective array element with its effective aperture in the coupled five-element array, and the two directors,  $D2_T$  and  $D2_B$  patches are considered as another single effective array element with its

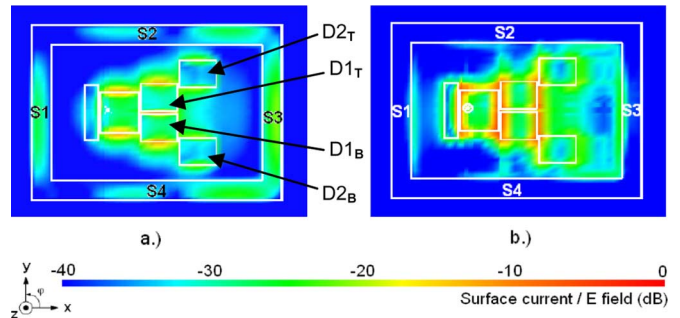


Fig. 2. Peak magnitude distribution of the SS microstrip Yagi array antenna at 5.8 GHz of (a) the surface current; and (b) the electric field intensity in the x-y plane at 1 mil above the metal patches' surface (63 mils above the ground plane).

effective aperture. The effective aperture of the two single effective array elements is demonstrated by the surface current distribution shown in Fig. 2(a). The operation of the five-element array is based on the coupling of the fringing field at the inner edge of the metal strip S1 (Fig. 2(a)) with the nearest radiating edge of the driven patch, and the coupling of the fringing field at the inner edge of the metal strip S3 (Fig. 2(a)) with the nearest radiating edge of the effective array element formed by the D2 patches. Even though the magnitude of the fringing field along the inner edges of the SS metal strips may be much lower than that of the antenna patches, the size of the ring is much larger than the patches so that the total fringing field along the

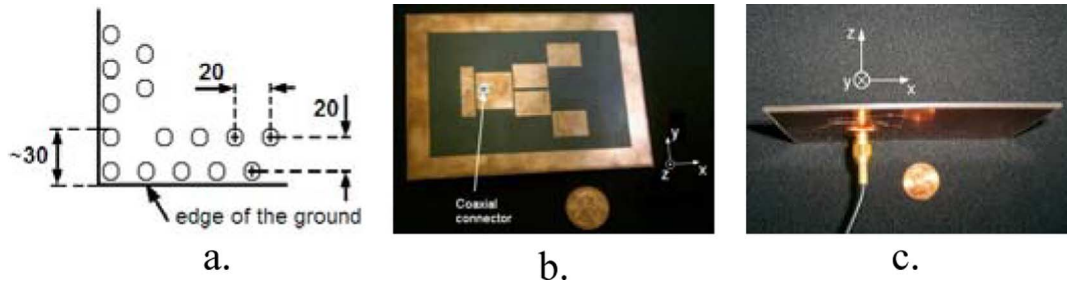


Fig. 3. (a) The top down view of the double via rows with all dimensions in mils. The soft-surface microstrip Yagi array antenna prototype showing (b) the front view and (c) the backside view.

metal strips (S1 and S3) exhibits constructive interference and becomes comparable to that of the patches; thus its effective contribution to the operation of the five-element array (in the E plane) is significant. This coupling effect can be observed directly from Fig. 2(b) where the electric field distribution is captured at the distance of 1 mil above the metal patches' surface in the z direction, showing the radiation field is strongly present at the inner edges of the metal strips S1 and S3. The inner width of the ring,  $W_s$ , becomes the factor that determines the size of the metal strips S1 and S3. Therefore, the spacing,  $g_{d2}$  is approximately  $0.4\lambda_o$ , and the spacing,  $g_r$  is approximately  $0.3\lambda_o$  (Fig. 1), while  $W_s$  is approximately one  $\lambda_o$ . As a result, the roles of the metal strips S2 and S4 are not as critical in this array coupling effect; however their length,  $L_s$  depends on the parameters  $g_{d2}$  and  $g_r$  which strongly affect the coupling. The soft surface ring does not allow the surface waves to be totally suppressed in all directions. This is because the soft surface ring is not a true surface-suppressing structure. A true surface-suppressing configuration has a periodic array of rings that blocks radiation as discussed in [10] and [11], but this makes the total size of the antenna very large. Hence, there is a tradeoff between size and total surface wave suppression. Despite this, the single soft surface ring does serve to improve the gain and F/B ratio.

It is important to note that the SS ring not only functions as a high surface impedance structure that blocks the surface wave, but also acts as a resonant structure that constructively supports the radiation of the Yagi antenna. In contrast to a conventional large-area artificial SS structure where the thickness of the slab determines the central operating frequency, the shorting of the metal strips in the modern SS structure provides the conditions for the high surface impedance and the operating frequency is determined by the strip width [12], not by the thickness of the substrate. When applied to the microstrip Yagi antenna arrays, the operating principles of the SS ring, as discussed earlier, explain how the radiation pattern can be improved for an arbitrary thickness of the substrate as well as for a significantly reduced ground size in comparison to the size required for the best radiation performance in conventional patch antennas [13], [14]. In the new configuration, the ground size is reduced without affecting the radiation performance of the SS microstrip Yagi array, thus leading to the compact design shown in Fig. 1.

#### IV. SIMULATED AND MEASURED RESULTS

The SS-Yagi antenna was fabricated on a double-sided copper (Cu) clad board of RT/duroid 5880 material ( $\epsilon_r = 2.2$ ,  $\tan \delta =$

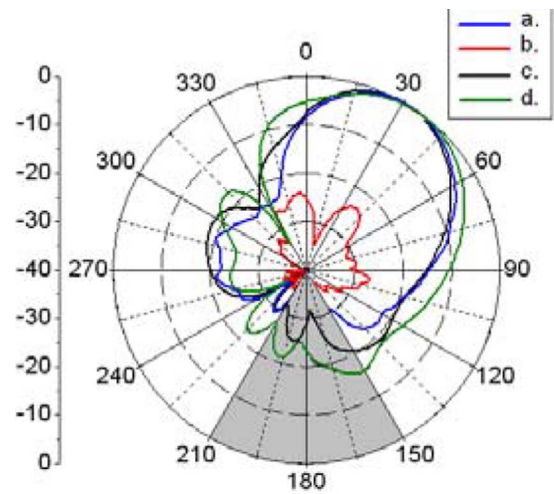


Fig. 4. Measured results of (a) copolarization and (b) cross-polarization in the range of  $-180^\circ \leq \theta \leq 180^\circ$  for SS-Yagi sample. Simulated results of copolarization in the range  $-180^\circ \leq \theta \leq 180^\circ$  for the (c) SS-Yagi model and (d) Non-SS-Yagi model.

0.0009) with a substrate thickness of 62 mils. The metal walls that short the metal strips of the SS ring to the ground are replaced by two rows of metal vias, with diameter and center-center separation equal to 10 mils and 20 mils, respectively. The double via rows are placed as indicated by the dash red line in Fig. 1 along the SS ring edge. The via rows with dimensions in mils are graphically shown in Fig. 3(a). Using vias in the prototype causes the choke length,  $Q_s$ , to decrease slightly. The distance from the ground edge to the edge of the inner via row is approximately 30 mils. To account for this decrease, the choke length,  $Q_s$ , has been increased to 362 mils to account for the presence of the vias. Therefore, an effective choke length equal to  $\lambda_g/4$  is maintained. The prototype of the SS-Yagi antenna is shown in Fig. 3(b) and (c). The simulated and measured E-plane radiation patterns at 5.8 GHz are shown in Fig. 4. The results of the non-SS model and SS model with the same configuration are compared. Here, the critical parameters that are considered are the sidelobe level (SLL) and the F/B ratio. The SLL refers to the ratio of maximum radiation in the range of  $270^\circ \leq \theta \leq 360^\circ$  (or  $0^\circ$  as shown in Fig. 4) to maximum radiation (normalized to 0 dB) in the range of  $0^\circ \leq \theta \leq 90^\circ$ . The measured SLL of the SS-Yagi antenna sample is  $-20$  dB, while the measured F/B ratio is 22 dB. The measurements were performed using an antenna measurement system where the first

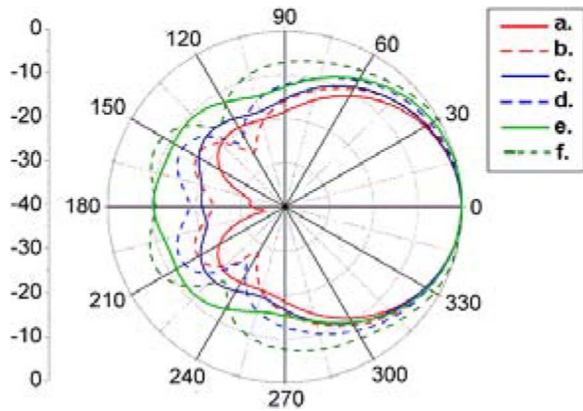


Fig. 5. Simulated  $E_\theta$  components of azimuth plane radiation ( $\theta = 90^\circ$ ) for the (a) SS model at 5.6 GHz; (b) non-SS model at 5.6 GHz; (c) SS model at 5.8 GHz; (d) non-SS model at 5.8 GHz; (e) SS model at 6.0 GHz; and (f) non-SS model at 6.0 GHz.

probe and the last probe leave a blind angle of about  $60^\circ$  corresponding to the shaded region in Fig. 4 ( $150^\circ \leq \theta \leq 210^\circ$ ). In measurement, the coaxial connector can act like a reflector that interferes with radiation in the region close to the connector (see Fig. 3(c)). This contributes to the difference between measured and simulated data in the region of  $135^\circ \leq \theta \leq 225^\circ$  shown in Fig. 4. Since the radiation immediate to the right of the coaxial connector (Fig. 3(c)) is expected to have stronger radiation than that to the left of the connector, the effect of the connector on the radiation in the region of  $130^\circ \leq \theta \leq 230^\circ$  is more pronounced; hence, the beam may be steered upward (in  $+z$  direction) which results in a lower peak compared to simulated results.

The cross polarization from the SS-Yagi antenna sample remains low. The increase in the cross-polarization is due to the coaxial line that is positioned off the center (in the  $y$ -direction) of the driven patch in order to achieve matching, thus introducing an asymmetry in the feed that generates higher order modes which contribute to cross-polarized radiation.

The suppression effect of the SS ring is also further illustrated in Fig. 5 where the  $E_\theta$  components of the azimuth plane radiation pattern ( $\theta = 90^\circ$ ) are shown at 5.6, 5.8, and 6.0 GHz. The suppression of the grating lobes due to the SS ring are shown through the decrease of the radiation levels at  $\varphi = 180^\circ$  as well as the lobes in the ranges of  $90^\circ \leq \varphi \leq 180^\circ$  and  $180^\circ \leq \varphi \leq 270^\circ$  with respect to the peak radiation at  $\varphi = 0^\circ$  for all three frequencies.

The return loss of the non-SS and SS models are shown in Fig. 6. The impedance bandwidth is taken at  $-10$  dB. It is observed through simulation that the impedance bandwidth of the SS models is similar to that of the non-SS model. In general, the SS models can be subjected to a decrease in the impedance bandwidth due to the fact that the SS ring is a highly frequency dependent structure (the optimized metal strip width,  $Q_s$ , is  $\lambda_g/4$ ). At frequencies off resonance, the SS ring cannot trap surface waves as effectively; thus, the quality (Q) factor due to space wave losses is increased. So it is important to note that the impedance bandwidth of the antenna is limited by the bandwidth of the SS ring, but the degree of limitation is determined by the performance specifications of the design and its application. For instance, as the lateral area of the SS ring is decreased,

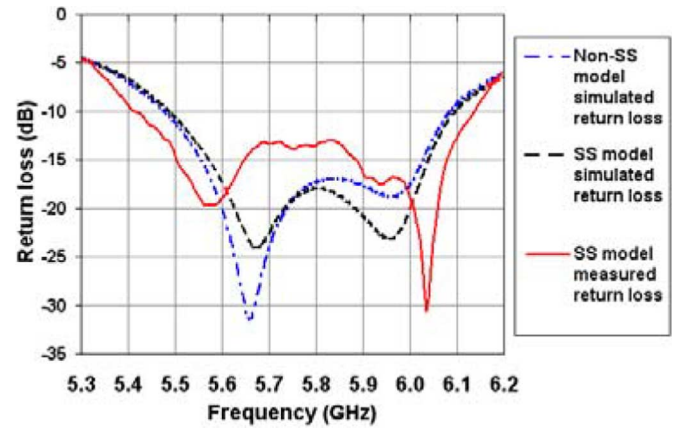


Fig. 6. Frequency response of the simulated and measured results (S11-Parameter) of non-SS and SS models with center frequency of 5.8 GHz.

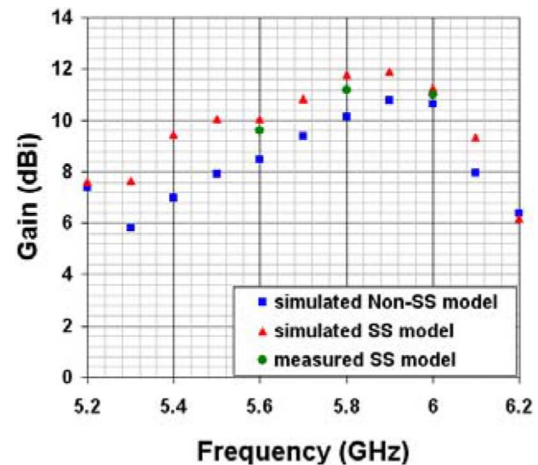


Fig. 7. Measured gain of the SS-Yagi sample.

the radiation pattern characteristics will be affected significantly because the SS ring will become closer to the near fields of the antenna and therefore, standing waves could arise. In addition, the impedance bandwidth could be adversely affected. In contrast, as the lateral area of the SS ring is increased, the effective aperture area increases leading to improved gain at the cost of potentially increasing the number of sidelobes in the pattern. As it is further increased, no performance-enhancing effect will take place at all.

The simulation results show an improvement of at least 3 dB in the F/B ratio (19.1 dB) compared to that of the non-SS model (16.1 dB), while a low SLL is maintained. The measured gain of the SS-Yagi sample was plotted in Fig. 7. The gain bandwidth is defined to be at the 10 dBi level which is around 10% for the SS-Yagi antenna.

## V. CONCLUSION

A new antenna structure based on surrounding a microstrip Yagi array antenna with an SS ring is demonstrated to exhibit highly directional radiation in which the F/B ratio are improved to more than 20 dB; this is approximately more than 3 dB higher than the conventional design without the ring. A high gain is achieved, while the size of the structure is reduced by a factor

of two. Although in a practical communications system where this antenna is connected to another component, presumably a filter, a F/B ratio of better than 20 dB may not be realized. The improvement in the 10 dBi directional bandwidth enables an almost constant directivity over a large bandwidth, thus allowing applications, such as wireless multimedia/HDTV devices to have more channels of signals without interference or degradation in signal quality. Finally, it has to be stressed that the SS technique proposed in this letter is a robust method that can be implemented on generic planar structures to suppress unwanted radiation, improve the directivity and the F/B ratio, and reduce the total size of the design.

#### ACKNOWLEDGMENT

The authors would like to thank Per O. Iversen, SATIMO USA, for supplying the microwave chamber in the antenna radiation measurement and acknowledge the support of the Georgia Electronic Design Center.

#### REFERENCES

- [1] C. A. Balanis, *Antenna Theory: Analysis and Design*, 2nd ed. New York: Wiley, 1997.
- [2] [Online]. Available: <http://www.manufacturers.com.tw/telecom/Yagi-Antenna.html>
- [3] [Online]. Available: <http://www.starantenna.com>
- [4] J. Huang, "Planar microstrip Yagi array antenna," in *Procs. IEEE Antennas Propag. Society Int. Symp.*, Jun. 1989, vol. 2, pp. 894–897.
- [5] A. Densmore and J. Huang, "Microstrip Yagi antenna for mobile satellite service," in *Proc. IEEE Antennas Propag. Society Int. Symp.*, Jun. 1991, vol. 2, pp. 616–619.
- [6] J. Huang and A. Densmore, "Microstrip Yagi antenna for mobile satellite vehicle application," *IEEE Trans. Antennas Propag.*, vol. 39, no. 7, pp. 1024–1030, Jul. 1991.
- [7] S. Padhi and M. Bialkowski, "Investigations of an aperture coupled microstrip Yagi antenna using PBG structure," in *Procs. IEEE Antennas Propag. Society Int. Symp.*, Jun. 2002, vol. 3, pp. 752–755.
- [8] D. Sievenpiper, L. Zhang, R. F. J. Broas, N. G. Alexopoulos, and E. Yablonovitch, "High-impedance electromagnetic surfaces with forbidden frequency band," *IEEE Trans. Microw. Theory Techn.*, vol. 47, pp. 2059–2074, Nov. 1999.
- [9] G. R. DeJean and M. M. Tentzeris, "A new high-gain microstrip Yagi array antenna with a high front-to-Back (F/B) ratio for WLAN and millimeter-wave applications," *IEEE Trans. Antennas Propag.*, vol. 55, no. 2, pp. 298–304, Feb. 2007.
- [10] R. L. Li, G. DeJean, M. Tentzeris, J. Laskar, and J. Papapolymerou, "LTCC multilayer based CP patch antenna surrounded by a soft-and-hard surface for GPS applications," in *Proc. IEEE Antennas Propag. Society Int. Symp.*, Jun. 2003, vol. 2, pp. 651–654.
- [11] P.-S. Kildal, "Artificially soft and hard surfaces in electromagnetics," *IEEE Trans. Antennas Propag.*, vol. 38, no. 10, pp. 1537–1544, Oct. 1990.
- [12] G. Ruvio, P.-S. Kildal, and S. Maci, "Modal propagation in ideal soft and hard waveguides," in *Proc. IEEE Antennas Propag. Society Int. Symp.*, Jun. 2003, vol. 4, pp. 438–441.
- [13] A. K. Bhattacharyya, "Effects of ground plane and dielectric truncation on the efficiency of a printed structure," *IEEE Trans. Antennas Propag.*, vol. 39, no. 3, pp. 303–308, Mar. 1991.
- [14] S. Noghianian and L. Shafai, "Control of microstrip antenna radiation characteristics by ground plane size and shape," *IEE Proc. Microw. Antennas Propag.*, vol. 145, no. 3, pp. 207–212, Jun. 1998.